Programmable Autonomous Micromixers and Micropumps

Abhishek K. Agarwal, Sudheer S. Sridharamurthy, David J. Beebe, *Member, IEEE*, and Hongrui Jiang, *Member, IEEE*

***Abstract*—Programmable autonomous micromixers and micropumps have been designed and realized via a merger between MEMS and microfluidic tectonics (μFT). Advantages leveraged from both fabrication platforms allow for relatively simple and rapid fabrication of these microfluidic components. Nickel (Ni) microstructures, driven by an external rotating magnetic field, are patterned *in situ* and serve as the microactuators in the devices. μFT permits *in situ* patterning through the use of a step-and-repeat fabrication process known as liquid-phase photopolymerization (LP^3). LP^3 is a polymer-based fabrication process tool that offers additional fabrication materials, including responsive hydrogels that expand and contract under different stimuli. Using pH- and temperature-sensitive hydrogels as clutches, autonomous micromixers and micropumps have been fabricated and tested that perform as closed-loop microsystems. The step-and-repeat fabrication process allows pre-programming of the system, like a programmable read-only memory chip, to be sensitive to a desired stimulus. Different Ni blade designs, and pH-sensitive hydrogel geometries and dimensions have been designed and tested to better ascertain their effects on micromixing efficiency and response times of hydrogels (related to the autonomous functionality), respectively. Temperature-responsive hydrogels have allowed for development of temperature-sensitive micromixers and micropumps with applications in areas demanding temperature control. [1498]**

***Index Terms*—Autonomous, magnetic actuator, micromixer, micropump, programmable.**

I. Introduction

MICROMIXERS and micropumps are essential components for fluidic handling in microfluidic systems [1], [2]. Numerous designs of micromixers exist and help facilitate the development of microfluidic systems for mixing at the microscale [3]–[11]. Likewise, a variety of micropumps have been developed based on different functioning methodologies [12]–[17]. Many of these systems require on-chip power, and costly and time-consuming (cleanroom) fabrication processing. Integrating these systems with other platforms, such as biological systems, often necessitates macro/micro assembling [18]. Furthermore, if the individual devices are extended to complete micro arrays systems, individual access and control of each singular device may prove to be difficult without additional on-chip wiring, power, and control systems. An example scenario is shown in Fig. 1(a). To combat these challenges, we present a first example of programmable autonomous micromixers and micropumps developed using a merger between IC-based MEMS (via fabrication and electroplating of nickel (Ni) structures) and microfluidic tectonics (μFT) processing.

We previously showed a first demonstration of *in situ* fabrication of autonomous micro actuators by leveraging advantages of both aforementioned fabrication platforms without micro/macro assembly of the two technologies [19], [20]. μFT uses liquid-phase photopolymerization (LP^3) of photosensitive polymers to rapidly create microcomponents [18], [21] without the need for a cleanroom. μFT offers additional (bio)compatible materials to work with, including responsive hydrogels. Responsive hydrogels exhibit volume changes depending on their sensitivity to a physical or chemical stimulus, such as pH [22]–[24], temperature [25], [26], light [27], pressure [28], biological agents [29], and electric fields [30], [31]. Here, the autonomous functionality of the micromixers and micropumps is achieved by exploiting the volume changes exhibited by pH- and temperature-responsive hydrogels. The transduction of chemical to mechanical energy, inherent to responsive hydrogels, is utilized to access and control the on/off status of a microcomponent in an array system. The responsive hydrogel functions similar to an automotive clutch. Using this platform merger, it is feasible to simplify the example scenario previously shown in Fig. 1(a) to (b).

Using the best from MEMS and μFT, a more extensive approach to *in situ* fabrication of programmable autonomous micromixers and micropumps, driven by an external rotating magnetic field, is presented here. Since volume changes for responsive hydrogels are diffusion-limited [32], [33], we attempt to study the potential of reducing the physical dimensions of the hydrogels, from macro- to microscale, which provides faster time responses. Autonomous micromixers with various hydrogel geometries and dimensions have been designed and tested to understand how size and geometry of hydrogels affect response time. Another attractive feature of this *in situ* fabrication process is the ability to define, or preprogram, each device on a single chip to be sensitive to a different physical stimulus (here, pH and temperature). Additional experiments on micromixing efficiency as a function of the Ni rotor's physical geometry have also been studied here.

Manuscript received January 10, 2005; revised June 22, 2005. This work was mainly supported by the Wisconsin Alumni Research Foundation (WARF) and partially by DARPA BioFlips program. The authors would like to thank the Wisconsin Center for Applied Microelectronics (WCAM) facility at the University of Wisconsin-Madison for cleanroom processing. Subject Editor C. Liu.

A. K. Agarwal, S. S. Sridharamurthy, and H. Jiang are with the Department of Electrical and Computer Engineering, University of Wisconsin-Madison, Madison, WI 53706 USA (e-mail: hongrui@engr.wisc.edu).

D. J. Beebe is with the Department of Biomedical Engineering, University of Wisconsin-Madison, Madison, WI 53706 USA.

Digital Object Identifier 10.1109/JMEMS.2005.859101

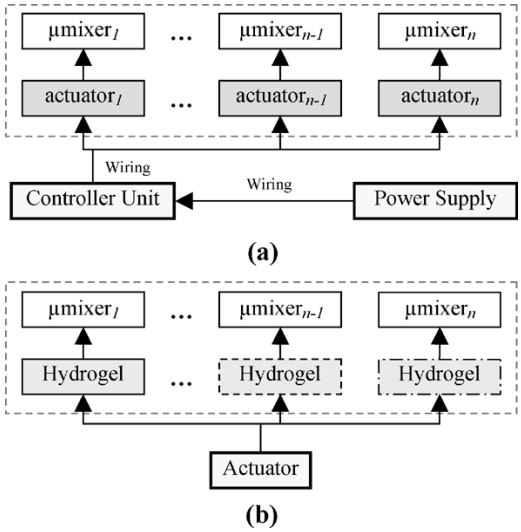

Fig. 1. An example scenario involving two designs of a micromixer array that provides individual control of which micromixer is activated and which is not. (a) Using traditional MEMS, a possible approach to designing a micromixer array. Individual actuators are required to control their respective micromixers, and thus, on-chip wiring, power, and control systems are necessary. (b) Combining MEMS and μFT, a more simplified solution that exploits the mechanical energy exhibited by responsive hydrogels. Here, one or more types of responsive hydrogels (indicated by the different style of box lines) can be used to design autonomous micromixers driven by a single actuator.

II. Photosensitive Polymers and Autonomous Functionality

The photosensitive polymers can be classified into two categories: nonresponsive and responsive. Non-responsive polymers do not react or respond to a change in stimuli, such as pH or temperature. These polymers serve as structural polymers, i.e., forming the body and structure (e.g., microchannels and posts) of the microsystems. However, responsive polymers (here, responsive hydrogels) exhibit change in volume due to a change in the local environmental stimulus. Here, pH- and temperature-sensitive hydrogels provide the programming capability of the device such that the microsystem will autonomously respond to a given local change in its environment without the necessity for on-chip wiring or electricity.

Photolithographic procedures are carried out using a desktop EXFO Acticure 4000 (EXFO Photonic Solutions, Inc., Mississauga, ON, Canada) ultraviolet (UV) light source. High resolution (3600 dpi) film photomasks (Silverline Studio, Madison, WI) are used to transfer patterns to the photosensitive polymers.

A. Nonresponsive Polymers

The nonresponsive photosensitive polymer used here, similar to negative photoresists, consists of three constituents in the following ratios: 31.66:1.66:1.0 $\rightarrow$ monomer—isobornyl acrylate (IBA), crosslinker—tetraethylene glycol dimethacrylate (TeGDMA, Sigma-Aldrich, St. Louis, MO, USA), and photoinitiator—2,2-dimethoxy-2-phenylacetophenone (DMPA, Sigma-Aldrich, St. Louis, MO, USA). Exposure to a UV light source causes the prepolymer solution to harden [called poly(IBA)]. It is also used as a mold for Ni electroplating.

B. Responsive Polymers

The responsive polymers, or hydrogels, are a three-dimensional (3-D) cross-linked polymeric network that swell and contract in aqueous solutions, depending on its inherent physical or chemical sensitivity [22].

1) pH-Sensitive Hydrogels: pH-sensitive hydrogels change their volume depending on the local environmental pH. Furthermore, they can be classified into hydrogels that expand in acidic solutions and those that expand in basic solutions. The former hydrogel [poly(DMAEMA-HEMA)] consists of four constituents in the following ratios [34]: 5.718:27.627:0.467:1.0 $\rightarrow$ pH-sensitive monomer—2-(dimethylamino)ethyl methacrylate (DMAEMA, Sigma-Aldrich, St. Louis, MO), inert monomer—2-hydroxyethyl methacrylate (HEMA, 0–50 ppm MEHQ inhibitor, Sigma-Aldrich, St. Louis, MO), crosslinker—ethylene glycol dimethacrylate (EGDMA, Sigma-Aldrich, St. Louis, MO), and photoinitiator—DMPA. It has a volume transition point of pH 6.5–7.0 [34]. The latter hydrogel group [poly(AA-HEMA)] is also made up of four constituents: 4.054:29.286:0.334:1.0 $\rightarrow$ pH-sensitive monomer—acrylic acid (AA, Sigma-Aldrich, St. Louis, MO), inert monomer—HEMA, crosslinker—EGDMA, and photoinitiator—DMPA. It has a volume transition point of pH 7.0 [34].

2) Temperature-Sensitive Hydrogels: These hydrogels exhibit a volume change that is dependent on local environmental temperatures, i.e., at low temperatures, it expands and at high temperatures, it contracts. A very common monomer used to fabricate temperature-sensitive hydrogels is N-isopropylacrylamide (NIPAAm) [22], [26]. The hydrogel consists of five constituents in the following ratios: 2.18:0.124:0.154:3.0:1.0 $\rightarrow$ temperature-sensitive monomer—NIPAAm (Acros Organics, Morris Plains, NJ), $\mathrm{N,N'}$-methylenebisacrylamide (NMBA, Acros Organics, Morris Plains, NJ), photoinitiator—DMPA, dimethyl sulphoxide, and deionized (DI) water. The hydrogel chemistry used here results in a volume transition point, commonly known as the lower critical solution temperature (LCST), of 30 °C. However, the recipe can be altered to create hydrogels with other transition temperatures [26], [35].

C. Autonomous Functionality

To achieve the aforementioned autonomous functionality in the microsystems, responsive hydrogel rings that will behave much like a clutch are patterned at the center axis of the electroplated Ni rotor. For example, consider a pH-sensitive poly(AA-HEMA) hydrogel ring that expands in basic solutions and shrinks in acidic solutions shown in Fig. 2. The Ni rotor is coupled with an underlying rotating magnetic stirrer that is constantly on. By lowering the local environment pH [see Fig. 2(a)], the hydrogel ring shrinks, allowing the Ni rotor to rotate freely; however, when the local pH is raised above its transition point [see Fig. 2(b)], the hydrogel ring expands. Previously reported [19], [20] as only a lateral expansion, it is now known that responsive hydrogels, in fact, expand into a mushroom cap shape as shown in Fig. 2(c).

Verification of the mushroom cap was obtained after experiments were conducted under the observation of a Nikon C1 Laser Confocal microscope (Nikon, Melville, NY;

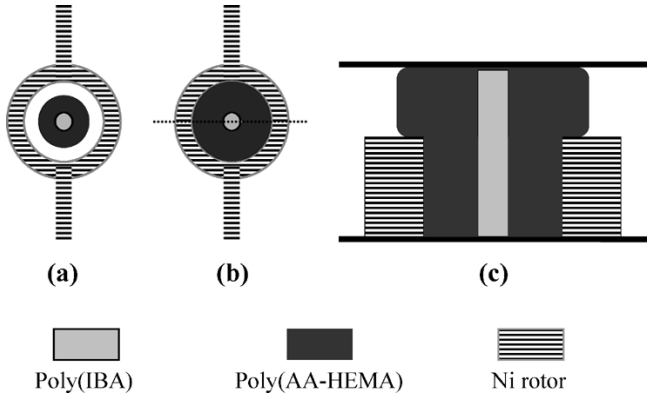

Fig. 2. Conceptual diagram of using poly(AA-HEMA) to control the actuation of a Ni rotor, much like an automotive clutch. (a) Low pH causes the hydrogel to shrink, allowing the Ni rotor to rotate freely. (b) High pH causes the hydrogel ring to expand in volume, constricting the Ni rotor's rotational movement. (c) A cross-sectional image of the expanded hydrogel, taken at the dotted line in (b) that shows the development of an overlaying mushroom cap on top of the Ni rotor.

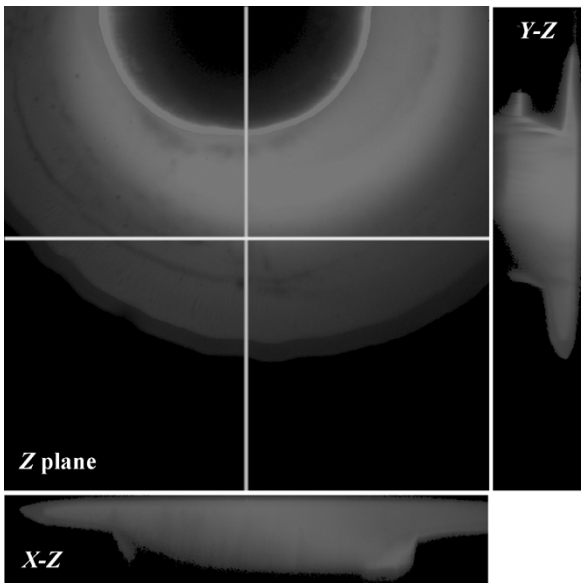

Fig. 3. Confocal imaging of a poly(AA-HEMA) hydrogel ring doped with Rhodamine B under the influence of high (10.0) pH buffer solution. It clearly shows the mushroom cap geometry taken on by the hydrogel that very likely creates both lateral and downward forces upon the Ni rotor.

Waisman Center at the University of Wisconsin-Madison). A poly(AA-HEMA) ring that had been previously doped with a very small amount of Rhodamine B, a fluorescent dye (excitation wavelength $= 555$ nm; emission wavelength $= 580$ nm), was photopatterned at the center axis of a Ni rotor. Hydrogels never revert back to their original photopatterned geometry once having gone through an expansion/contraction cycle; however, subsequent expansion/contraction cycles are very similar to each other. Thus, only after cycling through the hydrogel at least once, confocal imaging was done by alternately flowing in 0.05 M pH 2.0 and 10.0 (Fisher Scientific, Fair Lawn, NJ) buffer solutions. Fig. 3 shows the poly(AA-HEMA) hydrogel ring under the influence of high pH. The hydrogel ring takes on the shape of a mushroom cap [similar to the drawing show in Fig. 2(c)]. It is strongly believed the mushroom geometry exerts both lateral and downward forces on the Ni rotor, thereby causing the Ni rotor to stop rotating. Thus, the rationale for comparing the autonomous functionality using responsive hydrogels to a typical automotive clutch.

Using the step-and-repeat LP^3, a user can pre-program—like a programmable read-only memory (PROM) chip—microsystems to be autonomous to different physical stimuli (here, pH and temperature), all on the same chip. The fabrication process is general and the pre-programming can be accomplished by changing a single processing step. The fabrication process can be amended to change the autonomous programming (for example, from pH to temperature), as well as make it a nonautonomous microsystem.

III. Fabrication

The fabrication process leverages the advantages inherent to IC-based MEMS and $\mu\mathrm{FT}$ to design and develop the (autonomous) microsystems driven by an external magnetic stirrer. IC-based MEMS provides numerous advantages including standardization, high precision and accuracy, and microelectronics compatibility. These, merged with those offered by $\mu\mathrm{FT}$, present a solid foundation for the development of autonomous microfluidic systems. $\mu\mathrm{FT}$ uses LP^3 to create on-chip microenvironments on designated areas relatively quickly. Since it is accomplished in liquid-phase, it requires no spinning/casting of photosensitive materials and allows for self-planarization on substrates with varying topography. It is a low temperature ($< 100\ ^\circ\mathrm{C}$) platform that can act as a stand-alone or appended process. Furthermore, the merger continues to allow for a wide variety of substrates, including silicon, silicon nitride/oxide, and glass [19].

Ni electroplating is used to realize the magnetic components inside the microsystems that will couple with the external magnetic stirrer. The Ni structures are electroplated through a poly(IBA) mold. The *in situ* fabrication process utilizes a step-and-repeat approach to LP^3 where photosensitive polymers are used to define the body and structure, as well as the functionality of the (autonomous) devices.

A. General Fabrication of an Autonomous pH-Sensitive Micromixer

Here, microsystems are fabricated on precleaned microscope glass slides ($76.2\ \mathrm{mm} \times 25.4\ \mathrm{mm} \times 1.0\ \mathrm{mm}$, Fisher Scientific, Pittsburgh, PA). They are previously coated with thin layers of Ti/Cu/Ti (0.06/0.30/0.06 μm) using a CVC 601 DC sputterer. This is the single cleanroom step in this fabrication process. The bottom and top Ti layers serve to promote adhesion to the glass slides and prevent oxidation of the middle Cu layer, respectively. The Cu layer will serve as the future seed layer for Ni electroplating. Fig. 4 shows the fabrication process.

To define Ni structures on the glass slides, a poly(IBA) mold is patterned on the Ti/Cu/Ti-coated glass slides that will define the 2.5-dimensional structure of the Ni rotor. A cavity is created between the glass slide and film photomask of a Ni rotor (mask 1) using 225-μm-thick double-sided adhesive tape [see Fig. 4(a)]. The nonresponsive IBA-based prepolymer is

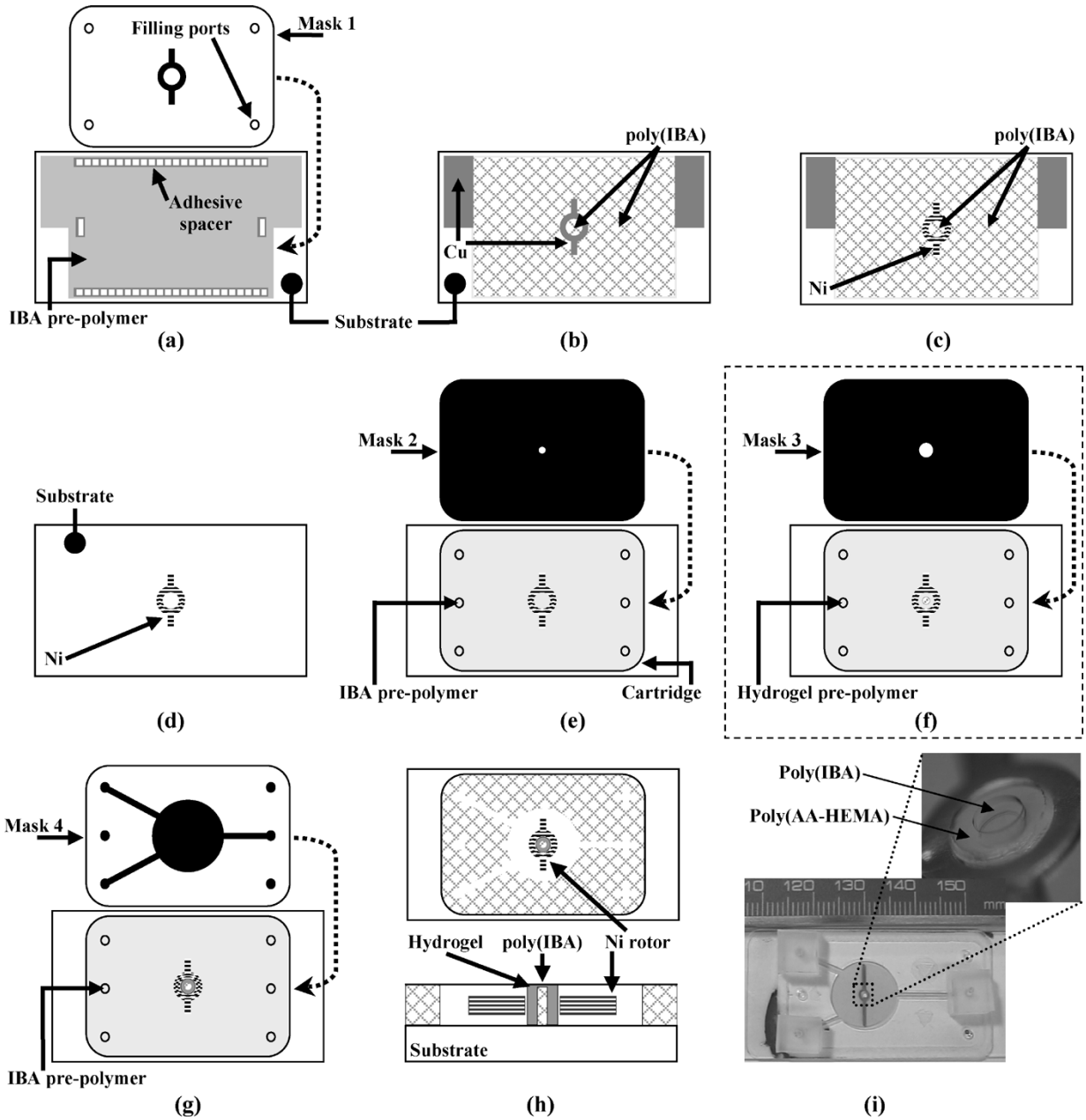

Fig. 4. General fabrication process flow (top view). Here, an autonomous pH-sensitive micromixer is fabricated. (a) A 225-μm cavity, created between the substrate (coated with Ti/Cu/Ti) and high-resolution film mask, is filled with the IBA-based pre-polymer mixture and exposed to UV light. (b) The top Ti-layer is removed, exposing the underlying Cu-layer. (c) Ni electroplating is performed with the poly(IBA) serving as the mold. (d) The poly(IBA) mold and seed metal layers are removed. (e) A polycarbonate cartridge is affixed to the substrate, creating a user-defined 250 or 375-μm cavity. The central core poly(IBA) post is photopatterned at the center axis of the Ni rotor. (f) An optional step that allows "preprogramming" the device to make it sensitive (and autonomous) to a physical stimulus [here, pH-sensitive using poly(AA-HEMA)]. A poly(AA-HEMA) hydrogel ring is photopatterned at the center axis of the Ni rotor. (g) The body and structure of the device (microchannels and mixing chamber) are defined and photopatterned inside the cartridge with poly(IBA). (h) The Ni rotor is released. A cross-sectional view (bottom) and top view of a functional and autonomous pH-sensitive micromixer. (i) Photograph of an autonomous (pH-sensitive) micromixer. Inset photograph shows the distinct central core poly(IBA) post and poly(AA-HEMA) ring.

flowed into the cavity using transfer pipettes and photopatterned by UVexposure (intensity, $I_{UV} = 7.7\ \mathrm{mW/cm^2}$; time, $t = 17.5$ s), rendering a negative image mold of the Ni rotor. The photomask is removed and the device is developed in a bath of ethanol (100%) for 180–240 s. The polymer mold definition step, from start to finish, takes under 10 min. Here, the unpolymerized prepolymer is rinsed away, leaving behind a hardened poly(IBA) mold of the Ni rotor. The device is softbaked on a hotplate at 50 °C for 15 min. To prepare the device for Ni electroplating at the active sites, i.e., where no poly(IBA) exists, the top Ti layer is removed using a 1:10 mixture of HF : H_2O (HF—technical grade, 48–50%, Fisher Scientific, Fairlawn, NJ, USA). See Fig. 4(b). The Ni electroplating bath, constantly agitated at 200 rpm, consists of 1:0.01 Microfab NI 100 make-up solution and Microfab NI 100 wetting agent (Enthone-OMI, West Haven, CT). The bath temperature, maintained at a temperature of $50\ ^\circ\mathrm{C} \pm 1\ ^\circ\mathrm{C}$, is constantly monitored by a type-K thermocouple probe. A high purity Ni gauze (#39704, Alfa Aesar,

Ward Hill, MA) is used as the Ni source for electroplating. Ni is electroplated onto the active sites on the glass slide (where Cu is exposed) at a rate of approximately 1.25–1.75 $\mu\mathrm{m/min}$ using a current density of 5×10^{-4} $\mathrm{A/mm^2}$ [36]. See Fig. 4(c).

Next, the poly(IBA) mold is removed by soaking the device in a 4:1 bath of methanol and acetone for several hours. The seed metal layers are also removed using 1:10 $\mathrm{HF : H_2O}$ for Ti removal and 1:1:10 $\mathrm{HAC : H_2O_2 : H_2O}$ (HAC—glacial HPLC grade; $\mathrm{H_2O_2}$—30%, Fisher Scientific, Fairlawn, NJ) for Cu removal [37]. See Fig. 4(d). A 22 mm × 40 mm polycarbonate cartridge (HybriWells, Grace Bio-Labs, Bend, OR, USA) that has an adhesive gasket film around the edge is placed on the glass slide, thereby containing the Ni rotor inside a thin cavity (250 or 375 $\mu\mathrm{m}$). The device is heated on a hotplate at 50°C for one min to activate the adhesive gasket and promote stronger adhesion to the glass slide. The IBA-based pre-polymer is flowed inside the cartridge through one of six filling ports using a transfer pipette. It is photopatterned through photomask 2 ($I_{UV} = 7.7$ $\mathrm{mW/cm^2}$; $t = 24.0$ s for 250 $\mu\mathrm{m}$ or 26.5 s for 375 $\mu\mathrm{m}$ cartridge) to create a small circular poly(IBA) post at the center axis of the Ni rotor [see Fig. 4(e)]. Ethanol is flushed through the cavity several times to remove the unpolymerized prepolymer. This central core poly(IBA) post serves many purposes, including increase in mechanical stability and reduction in the subsequent hydrogel ring width (improves the response time). The device is softbaked on a hotplate at 50 °C until all ethanol has evaporated from the cavity.

The next optional step serves to preprogram the microsystem to be sensitive to a certain physical stimulus, i.e., make the microsystem autonomous [see Fig. 4(f)]. The desired responsive hydrogel prepolymer is flowed into the cavity. It is similarly photopatterned (mask 3) at the center axis of the Ni rotor, forming an effective hydrogel ring around the central core poly(IBA) post. Here, as an example, a poly(AA-HEMA) ring ($I_{UV} = 10.0$ $\mathrm{mW/cm^2}$; $t = 64.0$ s) ring is photopatterned. The unpolymerized prepolymer is rinsed away with ethanol and subsequently softbaked on a hotplate at 50 °C until all ethanol has evaporated from the cavity.

The channels and body structure of the microsystem are defined last using the IBA-based prepolymer. Again, it is flowed into the cavity and photopatterned through mask 4 similarly [see Fig. 4(g)]. The Ni rotor is finally released from the glass slide by etching away the underlying sacrificial Ti and Cu layers [see Fig. 4(h)]. Initially, a 1:10 $\mathrm{HF : H_2O}$ mixture is flowed through the channel networks to etch away the bottom Ti layer, providing increased access to the Cu layer. Subsequent steps involve flowing in the Cu etching mixture repeatedly until the Ni rotor is released from glass slide. If there is any bottom Ti layer left on the glass slide, it is removed by briefly flowing in the Ti etching mixture. Fig. 4(i) shows a photograph of a completed micromixer with an inset photograph showing the central core poly(IBA) post and responsive hydrogel ring around it.

B. Access to the Microsystem

Connectors are fabricated to provide access to the microsystem and microchannels. In short, poly(dimethylsiloxane) (PDMS) slabs are constructed with an adhesive layer on the bottom to adhere to the filling ports on the polycarbonate cartridge.

A 3″ Petri dish is lightly sprayed with Duro All-purpose Spray Adhesive (Loctite Corp. North American Group, Rocky Hill, CT) to provide temporary support. One of the two liners of a 3″ circular disk of Secure Seal double-sided adhesive film (SA-S-1L, Grace Bio-Labs, Bend, OR) is removed and placed adhesive-side up inside the Petri dish. A 90 mm circular MicroSep cellulosic 5.0 $\mu\mathrm{m}$ filter (GE Osmonics Labstore, Minnetonka, MN) is placed on top of the sticky adhesive film already inside the Petri dish. A 1:10 Sylgard 184 silicone elastomer curing agent and Sylgard 184 silicone elastomer base (Dow Corning, Midland, MI) is prepared, placed in a dessicator, and vacuumed for 30 min to remove air bubbles. Next, it is slowly poured into the Petri dish and cured on a hotplate at 85 °C for 90 min to form a slightly elastic adhesive slab of PDMS. A sharp razor blade is taken to the edge of the inside of the Petri dish to remove the slab of adhesive, filter, and PDMS (bonded to one another) from the Petri dish. The slab is cut into desired sizes for connectors and a coring tool is used to create port holes through the three-layer connector. Next, the remaining adhesive liner is removed, and the connector port hole is aligned with and adhered to one of six filling ports on the polycarbonate cartridge. The microsystem is placed on a hotplate at 50 °C for 10 min to activate the adhesive and promote a stronger bond between the cartridge and PDMS connector. Microline tubing (I.D. = 0.51 mm; O.D. = 1.52 mm; Cole Parmer, Vernon Hills, IL) is routed inside the cored PDMS connector and permits delivery of any desired solution.

IV. Experiments and Results

For analysis and archival purposes, experiments are videotaped using a Sony Hyper HAD CCD-Iris/RGB camera (Sony Corporation, New York City, NY) that is mounted on an Olympus SZX12 stereoscope (Olympus, Melville, NY). When necessary, image analysis is performed using public domain NIH ImageJ 1.32j software. Here, an external rotating magnetic stirrer (Cole Parmer, model 84000-00, Vernon Hills, IL) is used to drive the microsystems. Since the length of the rotating magnet is approximately 5.0 cm (i.e., larger than the device size), a single magnetic stirrer can simultaneously drive multiple components fabricated on a single chip. To monitor the stirrer's rotational frequency, a small magnetic relay coil is attached to the stirrer and its outputs are connected to a HP 54600B 100 MHz oscilloscope (Hewlett Packard, Palo Alto, CA). Some experiments required the use of stable and controlled fluid flows into the microsystems and thus, syringe pumps were used (Cole Parmer, model 74 900 series, Vernon Hills, IL).

A. Ni Rotor Geometry Characterization

Previously, while demonstrating the ability to fabricate a variety of microactuators, including micromixers, preliminary experiments were done on a single four-blade micromixer to exhibit its micromixing efficiency at various input flowrates [19]. Here, multiple experiments were conducted that tested the effects of three Ni rotor blade dimensions to gain a more

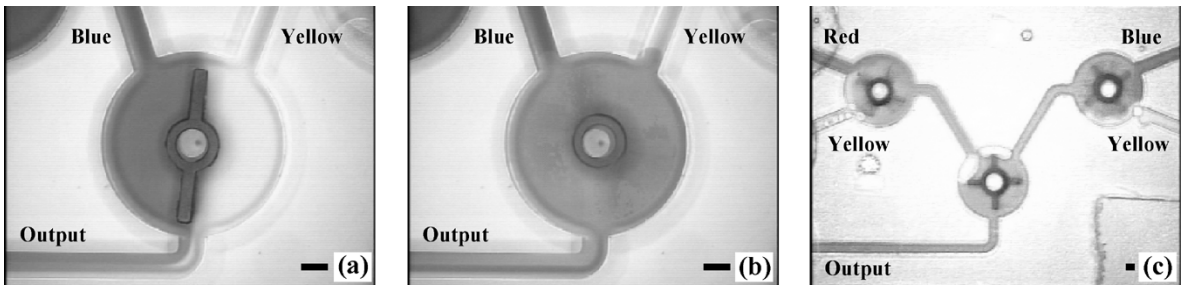

Fig. 5. Two photographs of a single micromixer (Ni rotor measuring $2.0\ \mathrm{mm} \times 0.40\ \mathrm{mm} \times 0.20\ \mathrm{mm}$) and one photograph of an array of three micromixers (Ni rotors measuring $1.5\ \mathrm{mm} \times 0.35\ \mathrm{mm} \times 0.20\ \mathrm{mm}$) with a central core poly(IBA) post. Scale bars represent 1.0 mm. (a) Using a syringe pump, the two input dyed water solutions (blue and yellow) flow into the system at an individual flowrate of $5.0\ \mu\mathrm{L/min}$. Laminar flow results at the output since the external magnetic stirrer is not activated, i.e., no mixing. (b) Upon activation of the magnetic stirrer, the Ni rotor rotates and causes chaotic action inside the mixing chamber, and subsequently mixes the two input fluids into a green output solution. (c) An array of three micromixers mixing dyed water solutions.

accurate perspective on micromixing efficiency: blade length, width, and thickness. The baseline geometry of the Ni rotor was kept to a length, width, and thickness of 2.0, 0.40, and 0.20 mm, respectively. This baseline geometry was modified as required to produce 11 distinct nonautonomous micromixers: five blade lengths (1–5 mm), three widths (0.20, 0.40, and 0.60 mm), and three thicknesses (0.125, 0.15, and 0.20 mm) were separately designed, fabricated, and tested. Microfluidic channels were 1.0 mm wide and 375 $\mu\mathrm{m}$ tall (defined by the cartridge). Using a syringe pump to administer the fluids, five total input flowrates—10, 250, 500, 1000, and 1500 $\mu\mathrm{L/min}$—were tested with each device. All experiments were conducted using a constant rotational magnetic stirrer frequency of 6.0 Hz.

It has been previously shown that micromixing efficiencies can be observed by mixing two colored fluids and subsequently evaluating the gray scale image intensities at the output channel [38]. Here, a similar approach has been applied by flowing two dyed water solutions into the input channels of the micromixer and observing the output channel. The blue input solution is comprised of a blue dye (FD&C Blue 1 food coloring) and DI water (0.015:1.0) while the yellow input solution is comprised of a yellow dye (FD&C Yellow 5 food coloring) and DI water (0.025:1.0). They are mixed inside the mixing chamber by active chaotic means due to the rotating Ni rotor, resulting in a green-colored solution at the output channel. A control experiment representing ideal mixing with intensity, I_0, is created for each device by flowing in a premixed Hy 1:1 blue:yellow-dyed solution. As an example of micromixing, Fig. 5(a) and (b) show a single Ni micromixer mixing blue and yellow input fluids into a green output fluid under the influence of an external magnetic stirrer. Fig. 5(c) shows an array of three Ni micromixers fabricated on the same chip mixing several different dyed water solutions. Here, a single external magnetic stirrer is shown to drive multiple components on a single chip, as described in Fig. 1(b).

The two input fluids were flowed into the device of concern using a single syringe pump. After a five second waiting period to allow the fluids to reach laminar flow, mixing was initiated by activating the external magnetic stirrer at 6.0 Hz and was kept on for a duration of 25 s. Once stopped, the device was allowed to reach laminar flow again. Gray scale intensities across the width of the output channel from acquired experimental images (I) were analyzed every two seconds for the last ten seconds of active micromixing, and subsequently compared with the ideal control mixing, I_0. The percent difference between the acquired experiment, I, and control, I_0, across the width of the output channel was determined using (1)

$$\text{Percent difference} = \frac{I - I_0}{I_0} \times 100. \tag{1}$$

Since the ideal control mixing I_0 will have a zero percent difference from (1), the slope of the percent difference across the channel width for I_0 will also be equal to zero. Hence, the slope of the linear regression from (1) was calculated for the experiments, where a $\text{slope} = 0$ (a constant gray scale intensity across the width of the output channel) exhibits highest mixing efficiency [10]. See Fig. 6 for the effects of Ni rotor geometry on mixing efficiency shown by the slope (absolute value) of the linear regression.

1) Blade Length: It is observed from Fig. 6(a) that longer blade length allows for more efficient mixing at higher input flowrates. Blade length 5.0 mm continues to maintain a mixing efficiency slope within 0.0–0.3 for all five flowrates whereas blade length 1.0 mm has a mixing efficiency that varies between 1.3 and 2.7. The extended blade length creates more active chaos inside the mixing chamber, thereby mixing the two input fluids with higher efficiency at higher flowrates.

2) Blade Width: Fig. 6(b) shows that an increase in the width of the Ni rotor blade accordingly increases the mixing efficiency. Whereas a width of 0.20 mm possesses a mixing efficiency ranging from 0.2 to 2.7, the 0.60 mm blade width consistently accomplishes higher mixing efficiency (slope between 0.3 and 1.0).

3) Blade Thickness: Fig. 6(c) suggests that an increase in blade thickness may in fact prevent efficient mixing since 0.20 mm thick blades perform at a lower efficiency when compared to both of the thinner Ni rotor blades at all tested flowrates. It is only comparable at total input flowrates of 10 and 1500 $\mu\mathrm{L/min}$. One feasible explanation is that the thinner blade not only rotates in the $x - y$ plane, but also oscillates in the z direction, thereby increasing the active chaotic mixing. This was visually observed during the experiments. As noted earlier, the height of the chamber is 375 $\mu\mathrm{m}$, and the thinner blades may indeed oscillate up and down along the poly(IBA) post and mix the two input fluids with comparable efficiency. The thicker blades, due to their additional weight, may only provide mixing by rotating in the $x - y$ plane.

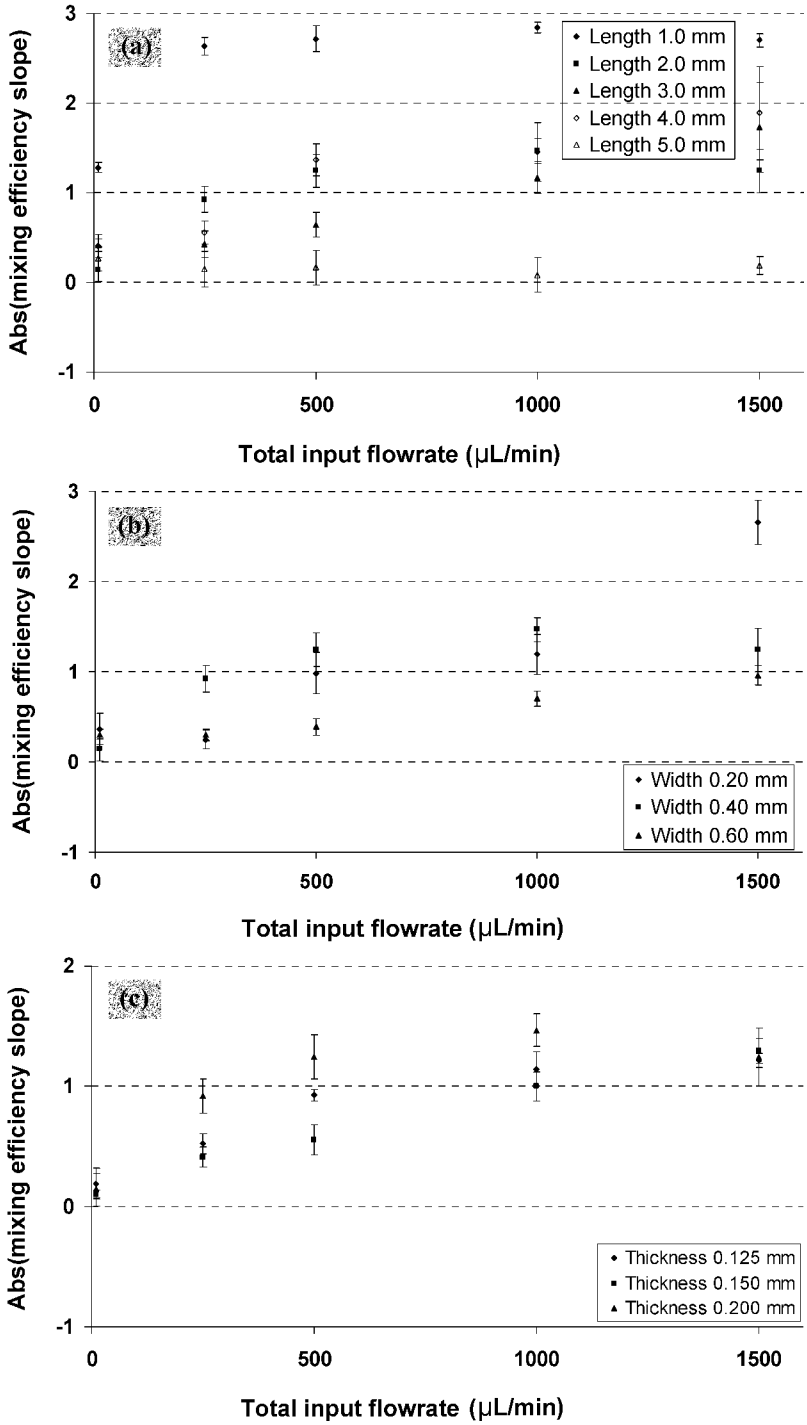

Fig. 6. Effect of three Ni rotor blade geometries on micromixing efficiency as a function of total input flowrate. Here, the absolute value of the slope is reported. A $\mathrm{slope} = 0$ represents ideal and most efficient mixing. The vertical bars for each data point represent standard deviation. (a) Ni rotor blade length. (b) Ni rotor blade width. (c) Ni rotor blade thickness.

B. pH-Sensitive Micromixers

Previously, pH-responsive micromixer arrays driven by a single external magnetic stirrer were developed with a photopatterned poly(AA-HEMA) ring at the center axis of each Ni rotor [19]. By simply changing the local environmental pH, one can choose, control, and determine which of the individual micromixer(s) rotate(s) and mix(es). This was accomplished by manually flowing in 0.05 M pH 2.0 and 10.0 buffer solutions into the devices to change the local pH of an individual micromixer, where an acidic solution would permit rotation and a basic solution would forbid rotation, previously shown in Fig. 2. Response times—the time taken for the Ni rotor to start or stop moving, depending on local pH—were reported on the order of tens of seconds [19]. Since volume transition of responsive hydrogels is a diffusion-limited process, reducing the dimension of the hydrogel should make it feasible to achieve faster time responses.

This very scenario was tested here—three separate autonomous micromixer devices were developed, each with a

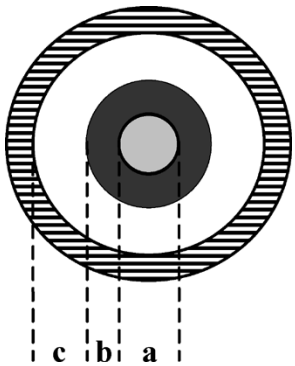

Fig. 7. Dimensions of the circular central core poly(IBA) post, and dimensions and geometry (ring or post) of the poly(AA-HEMA) hydrogel. Dimension c, the gap between the photopatterned hydrogel and inner body of the Ni rotor, was minimized as much as possible. Devices 1–3 have a poly(AA-HEMA) ring geometry. Control device 4 has no poly(IBA) post, but instead a single circular poly(AA-HEMA) post.

TABLE I
FABRICATED POLYMER POST DIMENSIONS

	'a'– poly(IBA) diameter (mm)	*'b'*– poly(AA-HEMA) ring width (mm)
Device 1	0.90	0.125
Device 2	0.70	0.225
Device 3	0.50	0.35
Device 4	—	1.15 diameter

different dimension of poly(AA-HEMA) ring, i.e., the $x - y$ plane dimension of the poly(AA-HEMA) ring was modified. See Fig. 7 and Table I for a schematic and numerical representation of the fabricated designs. Measurement c, the gap between the inside of the Ni rotor axis and the outside of the poly(AA-HEMA) hydrogel shown in Fig. 7, was minimized to the smallest extent feasible using the Olympus SZX12 stereoscope for photomask alignment. Poly(AA-HEMA) was photopatterned using $I_{UV} = 10\ \mathrm{mW/cm^2}$ and $t = 74.0$ s. Accordingly, the central core poly(IBA) post diameter was modified such that the poly(AA-HEMA) ring was always flush against the central core post. For control measures, a fourth micromixer device was fabricated that contained only a singular poly(AA-HEMA) post, i.e., no poly(IBA) central core post. Since the poly(AA-HEMA) rings are less wide than a solid hydrogel post (similarly stated, a larger ratio of exposed surface area to volume), the response times of the ring devices are expected to be comparably shorter, again since expansion/contraction of the hydrogel is a diffusion-limited process.

It was previously mentioned that hydrogels do not revert to their original photopatterned geometry once having gone through a volume expansion/contraction cycle. Thus, prior to performing experiments on the four given devices, they were alternatively exposed to pH 2.0 and pH 10.0 buffer solutions for at least two complete cycles. For each device, a single experimental session with nine trials was conducted where dyed 0.05 M buffer solutions ($\mathrm{pH} = 2.0 \rightarrow 0.008 : 1.0$ FD&C Blue 1:pH 2.0 buffer; $\mathrm{pH} = 10.0 \rightarrow 0.02 : 1.0$ FD&C Yellow 5:pH 10.0 buffer) were manually flowed into the device alternatively. One trial consists of the following: flowing in a low pH solution; waiting for the Ni rotor to rotate freely; flowing in a high pH solution; lastly, waiting for the Ni rotor to stop rotating completely. Experiments were videotaped and time responses were analyzed.

Two critical time groups were defined and observed—the "hydrogel response time" (HRT) and "Ni rotor response time" (NiRRT). The average time responses of all nine trials for each device are shown in Fig. 8. HRT(1) and (2), and NiRRT(1) and (2) are defined in the Fig. 8 caption. Fig. 8 shows the effect of hydrogel geometry and dimension on time responses.

Analysis of the data showed that diffusion is not the only parameter that affects the autonomous function of the devices here. But, the forces created by the responsive hydrogels and subsequently exerted on the Ni rotors also play an important role in the response time and behavior of the four tested devices. Diffusion, of course, is a critical component in allowing the ionic charge transfers to occur during volume transition; however, since the hydrogels here are being used similar to an automotive clutch, [hydrogels] must be able to exert enough force to start/stop the rotation. The geometry and dimension of the hydrogels impact the generated force. Realizing that diffusion is not the only parameter of concern was first observed from the HRT data.

Examining HRT(1), the data suggest and support the theory that thinner hydrogels provide faster time responses. All three hydrogel rings respond faster or comparable within their standard deviation limits when compared to the solid hydrogel post. Amongst the ring-based devices, the HRTs generally decrease with the increase of the hydrogel ring width (taking into consideration the standard deviations—SDs). However, when observing the data from HRT(2), it is the hydrogel post that seems to respond the fastest, instead of the hydrogel rings (precise statements about this observation cannot be made because of the SD variation). Considering diffusion alone, it is naturally expected that the hydrogel rings will perform faster. But, this is not the observation.

In addition to diffusion, there is another equally important parameter in the autonomous device behavior and the HRT data supports that this parameter is the exerted force (both lateral and downward) by the hydrogel. Fig. 2 previously discussed the basic mechanism by which the hydrogel takes on the shape of a mushroom cap and behaves as a clutch. Thinner hydrogel rings, although possessing faster diffusion times, are not able to produce the necessary forces to control the Ni rotor actuation. Instead, it takes them a longer time to develop the necessary force, thus resulting in longer HRTs. Additionally, having a thinner geometrical width allows limited expansion, i.e., a limitation in the size of the mushroom cap. A wider hydrogel ring, on the other hand, may have a slower diffusion time, but compensates by producing the effective and necessary force at a faster rate to control the actuation of the Ni rotor. The data strongly infers the existence of a critical hydrogel ring width that will provide optimal HRTs (and NiRRTs).

Examination of the NiRRT data also supports the claim that exerted force is an important parameter as well as the existence of an optimal hydrogel ring geometry. The thinnest hydrogel ring (width 0.125 mm) exhibits the longest time response when compared to the other two hydrogel ring widths. The solid post takes the longest time of all since diffusion is the limiting factor.

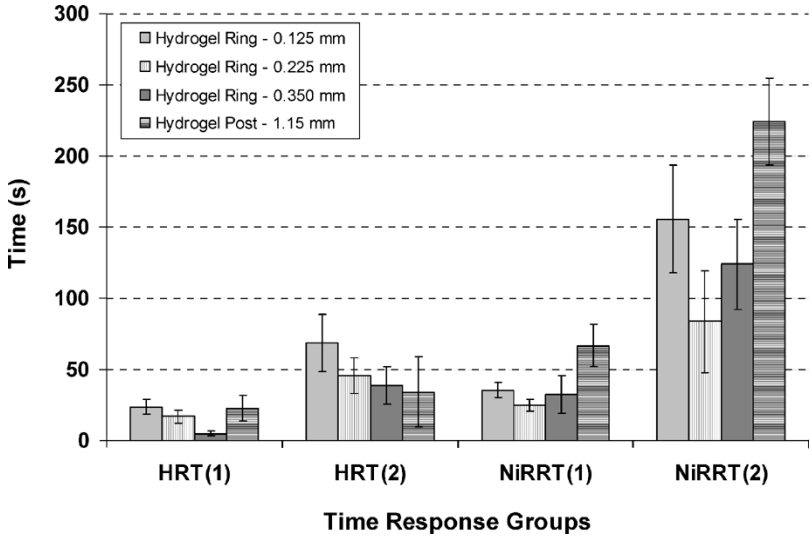

Fig. 8. Average of the critical time response analysis of four different poly(AA-HEMA) devices. Vertical bars represent standard deviation within the average of nine trials. HRT(1)—time difference between smooth rotor rotations to erratic rotations after influx of high pH buffer. HRT(2)—time difference between a completely stopped rotor to the slightest movement after influx of low pH buffer. NiRRT(1)—time difference between smooth rotor rotations to a completely stopped rotor after influx of high pH buffer. NiRRT(2)—time difference between a completely stopped rotor to smooth rotor rotations.

Hydrogel widths 0.225 and 0.35 mm, and the solid hydrogel post are fully capable of generating the necessary force in short time. Therefore, it is diffusion which becomes the dominating factor here. This provides an explanation why the 0.35 mm hydrogel ring responds slightly slower compared to the 0.225 mm hydrogel ring.

Due to equipment limitation, there is some variation in distance c (see Fig. 7) between all four devices despite attempts at minimizing the gap with the available equipment. If the gap is large, then the poly(AA-HEMA) hydrogel must expand in its size and geometry by larger dimensions compared to devices where c is smaller. Realizing a larger size and geometry takes time and may account for some of the delayed responses observed in the data, especially for the HRT analysis.

C. Poly(AA-HEMA) and Poly(DMAEMA-HEMA) Devices

Another advantage of this hybrid fabrication process is exploiting the step-and-repeat LP^3 process to define which devices, on a single chip, respond to which user-defined stimuli, i.e., preprogram the individual device to be sensitive to pH, temperature, etc. We demonstrate here the fabrication and testing of a single micromixer array chip that consists of three individual micromixer, where two of the three micromixers are fabricated with poly(DMAEMA-HEMA) hydrogel rings, and the last micromixer is fabricated with a poly(AA-HEMA) hydrogel ring. Here, under the constant presence of a rotating magnetic field, a low pH buffer solution should cause the poly(AA-HEMA) hydrogel ring to shrink and allow the Ni rotor to rotate, whereas the poly(DMAEMA-HEMA) hydrogel rings will expand and prevent Ni rotor rotation. Under the influence of a high pH buffer solution, the opposite effects should result.

The fabrication process is similar to the one described in Fig. 4. The process step described in Fig. 4(f) was repeated twice—patterning the single poly(AA-HEMA) hydrogel ring ($I_{UV} = 10\ \mathrm{mW/cm^2}$; $t = 74.0$ s), and patterning the two poly(DMAEMA-HEMA) hydrogel rings ($I_{UV} = 20\ \mathrm{mW/cm^2}$; $t = 49.0$ s). After patterning each specific hydrogel ring, the device is rinsed several times with ethanol, placed on the hotplate at $50^{\circ}\mathrm{C}$ until all the ethanol has dried from the polycarbonate cartridge cavity, and allowed to cool to room temperature prior to the next LP^3 process. Devices were patterned such that the central core poly(IBA) post has a diameter of 0.80 mm (measurement a in Fig. 7) and each of the two hydrogel rings has an effective width (measurement b in Fig. 7) of 0.225 mm.

Once the three Ni rotors were released and the connectors were attached, the hydrogels were cycled through the initial expansion/contraction phase. Once finished, the micromixer array was placed on top of the constantly rotating magnetic stirrer set at 6.0 Hz. Initially, a low pH buffer solution was manually flowed into the device such that all three micromixers were exposed to a low pH environment. Fig. 9(a) shows a photograph of two of the three micromixers where the top-left micromixer contains the poly(DMAEMA-HEMA) hydrogel ring and the bottom-right micromixer contains the poly(AA-HEMA) hydrogel ring. It shows the bottom-right micromixer rotor rotating smoothly, while the top-left micromixer sits still, despite the presence of the rotating magnetic field. Here, the poly(AA-HEMA) hydrogel ring is in a shrunken state and allows the Ni rotor to rotate freely; however, the poly(DMAEMA-HEMA) hydrogel ring is in an expanded physical state and prevents the rotor from rotating. After a few moments, the high pH buffer solution is flowed into the system, exposing both micromixers to the high pH buffer. During the changeover, there is a short period where both rotors rotate together [see Fig. 9(b)]. However, after some time, the poly(DMAEMA-HEMA) hydrogel ring shrinks sufficiently to allow the top-left rotor to rotate freely, while the poly(AA-HEMA) hydrogel ring expands to stop the bottom-right rotor's movement [see Fig. 9(c)]. This experiment was repeated once more with the same observed results. It should be noted here that during the changeover from high pH

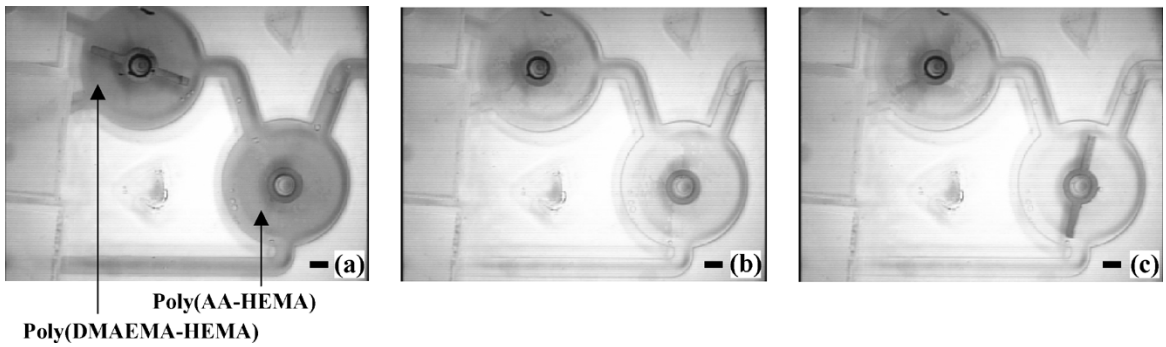

Fig. 9. Three photographs of two micromixers on a single chip. The top-left Ni rotor has been fabricated with a poly(DMAEMA-HEMA) hydrogel ring while the bottom-right Ni rotor has been fabricated with a poly(AA-HEMA) hydrogel ring. Scale bars represent 1.0 mm. (a) With a low pH buffer solution, the bottom-right micromixer freely rotates, while the top-left does not due to the expanded poly(DMAEMA-HEMA) hydrogel ring. (b) With the influx of a high pH buffer solution, the poly(DMAEMA-HEMA) hydrogel ring shrinks enough to allow the rotor to rotate freely. During this pH changeover, both rotors rotate freely for a brief period. (c) After a short time, the poly(AA-HEMA) hydrogel ring expands sufficiently to stop the rotor's rotation leaving behind the top-left device rotor to rotate on its own.

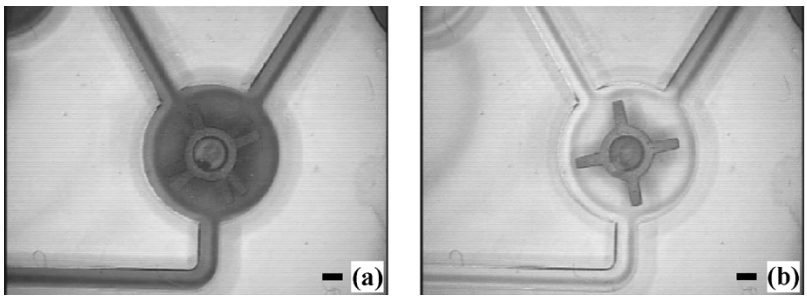

Fig. 10. Four-blade Ni rotor showing the feasibility of controlling fluid mixing at the microscale using poly(NIPAAm) hydrogel rings. Scale bars represent 1.0 mm. (a) In-flow of warm water causes the poly(NIPAAm) ring to shrink, allowing the four-blade Ni rotor to rotate freely. (b) In-flow of cold water causes the hydrogel ring to expand, thereby stopping the rotor's movement.

to low pH, both concerned rotors did not rotate together. The poly(DMAEMA-HEMA) hydrogel ring always expanded and stopped the Ni rotor's rotation before the poly(AA-HEMA) hydrogel ring shrunk sufficiently and allowed free rotation of the bottom-right rotor.

Using LP^3, two micromixers have been designed and fabricated on the same chip that accordingly behave contradictory to one another. The versatility of the step-and-repeat LP^3 fabrication process allows the fabrication of two or more different autonomous hydrogels on the same chip. Such ease of fabrication can open doors to development of a variety of other microsystems, each with the freedom to be tuned to a specific stimulus as defined by the fabricator.

D. Temperature-Sensitive Actuators

Several types of temperature-sensitive microactuators have been developed [22], [25], [26]. Using the merged fabrication techniques, micromixers and smart micropumps driven by an external magnetic rotating field have been designed and fabricated that respond autonomously to the local environmental temperature [20].

Temperature-responsive micromixer arrays were fabricated using the same process flow (see Fig. 4) except a poly(NIPAAm) hydrogel ring is patterned instead ($I_{UV} = 9.5\ \mathrm{mW/cm^2}$; $t = 15.2\ \mathrm{s}$). Fig. 10 shows two photographs of a four-blade single micromixer that responds to the local temperature changes and accordingly, controls the actuation of the Ni rotor in the presence of an external rotating magnetic field [20]. When warm fluid ($\sim 30^\circ\mathrm{C}$ or higher) is flowed through the channels [see Fig. 10(a)], the poly(NIPAAm) hydrogel ring shrinks and allows the Ni rotor to spin freely; however, when cold fluid ($< 26\ ^\circ\mathrm{C}$) is flowed through the channels [see Fig. 10(b)], the hydrogel ring expands within a short period of time and prevents the rotor's rotation. Here, the time responses of starting and stopping range between 3–12 s.

Smart micropumps, based on the concept of recirculation, that autonomously decide when and when not to pump fluid were also designed and fabricated using the same fabrication techniques. Because of the rotating actuation of the Ni rotor inside the device, a change in pressure is created within the microchannel, thus creating the force that drives the pumping mechanism [17]. Fig. 11 shows time-series photographs of a smart micropump. Initially, warm (slightly above 30 °C) DI water flows and pumps through the device. A drop of concentrated FD&C Yellow 5 food dye is introduced at the input filling port ($t = t_0$). It is slowly pumped through the device in a counterclockwise path [see Fig. 11(a)]. At $t_1 = t_0 + 5\ \mathrm{min}\ 15\ \mathrm{s}$, cold water (below 20 °C) is repeatedly introduced at the input filling port [see Fig. 11(b)]. At $t_2 = t_1 + 7\ \mathrm{min}\ 29\ \mathrm{s}$, enough cold water has been pumped through the smart micropump system to expand the poly(NIPAAm) hydrogel sufficiently to autonomously stop the pumping mechanism [see Fig. 11(c)].

Two different Ni rotor geometries were tested—four straight blades measuring $1.5\ \mathrm{mm} \times 0.35\ \mathrm{mm} \times 0.175\ \mathrm{mm}$ and four curved blades measuring approximately $1.37\ \mathrm{mm} \times 0.36\ \mathrm{mm} \times 0.175\ \mathrm{mm}$. Fig. 12 shows the image of each blade geometry and Table II lists the resulting flowrates and pressure gradients created from the pumping action. The constant rotating magnetic

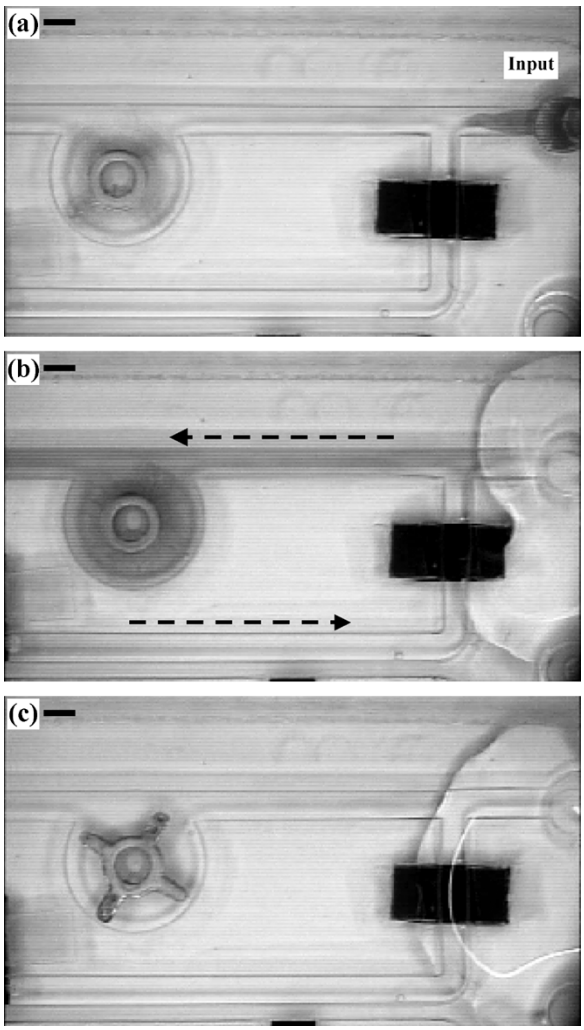

Fig. 11. Smart temperature-controlled micropump. The poly(NIPAAm) post expands and contracts, indirectly controlling the pumping action of the fluid. Scale bars represent 1.0 mm. (a) Warm water circulates through the channels. A drop of yellow dye is placed at the input. (b) The dye has been pumped to the left on the top channel (shown by top dashed arrow) and recirculated back along the bottom channel to the right (shown by bottom dashed arrow). Cold water is placed at the input. (c) The micropump stops pumping once the hydrogel expands sufficiently.

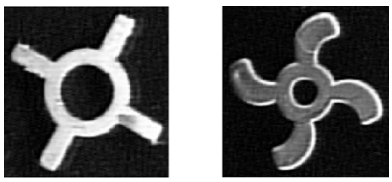

Fig. 12. Two Ni rotor geometries tested with the smart micropump. Device 1 consists of four straight blades measuring $1.5\ \mathrm{mm} \times 0.35\ \mathrm{mm} \times 0.175\ \mathrm{mm}$. Device 2 consist of four curved blades measuring $1.37\ \mathrm{mm} \times 0.36\ \mathrm{mm} \times 0.175\ \mathrm{mm}$.

TABLE II
RESULTING FLOWRATES AND PRESSURE GRADIENTS

	Flowrate (μL/min)	Pressure Gradient (Pa)
Device 1 – straight blades	1.53	0.355
Device 2 – curved blades	3.07	0.712

field is set at a rotational frequency of 51 Hz. Using ImageJ, flowrates were calculated by analytically tracking the flow of the dye over a prescribed distance during a period of time using (2) [17].

$$\text{flowrate} = h \cdot \frac{\Delta A}{\Delta t}. \tag{2}$$

Here, h is the height of the channel (here, 375 μm), ΔA is the increment of the dye over the observed area in two consecutive images, and Δt is the time difference between the consecutive images. Pressure, P, gradients were calculated using (3) and (4) [17].

$$P = flowrate \cdot R \tag{3}$$

$$R = 12 \cdot \frac{\mu \cdot L}{w \cdot h^3}. \tag{4}$$

Here, R is the resistance of the channel to the flow, $\mu = 0.001\ \mathrm{Kg} \cdot \mathrm{m}^{-1} \cdot \mathrm{s}^{-1}$ is the kinematic viscosity of water, L is the length of the channel in the loop (here, 61.18 mm), and w is the width of the channel (here, 1.0 mm).

These initial trials show that the curved blade rotor creates a higher flowrate (3.07 $\mu\mathrm{L/min}$) compared to the straight blade rotor (1.53 $\mu\mathrm{L/min}$). The curvature may in fact pull in more water from the input filling port and push it to the left [as shown in Fig. 11(b)] in a counterclockwise motion. Adding more rotors in series may provide faster flowrates. Further studies are needed to better understand this pumping mechanism, as well as how various parameters (e.g., rotor geometry and dimensions, channel width and thickness, number of rotors, and hydrogel geometry and dimension) affect the performance of the autonomous temperature-controlled micropump.

Both microactuators function as self-sustaining, closed loop temperature-sensitive devices without the need for on-chip wiring or electricity. Temperature-sensitive autonomous actuators have tremendous potential in microfluidics, especially in areas where temperature control is desirable.

V. CONCLUSION

Using the best from MEMS and μFT processing, autonomous micromixers and micropumps have been designed, fabricated, and tested. The technology enables preprogramming of devices on a single chip to be sensitive to either a single physical (or chemical) stimulus or expand it to multiple sensitivities, by taking advantage of responsive hydrogels (here, pH- and temperature-responsive). As an initial attempt to understand micromixing efficiencies, a variety of Ni rotor dimensions were fabricated and tested at different total input flowrates. Also, pH-responsive micromixers with various hydrogel geometries and dimensions have been designed and tested. They offer more insight into using hydrogels like automotive clutches. Not only does diffusion play a key role in the response time of the hydrogel and autonomous functionality of the device, but so does the force created inside the hydrogel and subsequently exerted on the Ni rotor.

Additionally, using the step-and-repeat approach to LP^3 processing, there is freedom to choose the sensitivity associated with each individual device. As an example, two micromixers with different pH sensitivities were realized here. Combining MEMS

and LP^3 provides a relatively fast approach to realizing micro actuators by eliminating costly cleanroom processing, spinning/casting of photosensitive materials, and providing a larger variety of plausible materials that may be used for fabrication. All of these have compounded the fabrication process into realizing a variety of micro actuators, including autonomous temperature-sensitive micromixers and micropumps that have potential for any applications where temperature control is desired.

Many further studies remain to be done. Here, an external magnetic stirrer was used to drive the system; further studies on the effect of rotational frequency on mixing efficiency and pumping rate are planned. Furthermore, it would be desirable to integrate a local actuator, such as a three-phase micromotor [7] to remove the necessity of an external driver. Also, studying different Ni rotor blade geometries would allow for observations of optimal micromixing and micropumping efficiency. Autonomous functionality is a key feature of these devices. Many further studies with a wider array of hydrogel geometries need to be studied to better ascertain their impact on the autonomous functionality of micro actuators. Designing and developing optimal responsive hydrogels will serve to promote faster time responses, opening more doors to potential applications.

ACKNOWLEDGMENT

The authors also recognize Ruth Sullivan and Carol Gabel at the Waisman Center at the University of Wisconsin-Madison for their assistance in confocal imaging. In addition, authors are grateful to Dr. J. Atencia (NIST), T. M. Pearce (Washington University, St. Louis, MO), and Dr. L. Dong (Electrical and Computer Engineering, University of Wisconsin-Madison) for their technical assistance and consultation in this work.

REFERENCES

[1] C. J. Campbell and B. A. Grzybowski, "Microfluidic mixers: from microfabricated to self-assembling devices," *Phil. Trans.: Math., Phys. Eng. Sci.*, vol. 362, pp. 1069–1086, May 15, 2004.

[2] N.-T. Nguyen, X. Huang, and T. K. Chuan, "MEMS-micropumps: a review," *J. Fluids Eng.*, vol. 124, pp. 384–392, 2002.

[3] X. Zhu and E. S. Kim, "Microfluidic motion generation with acoustic waves," *Sens. Actuators A, Phys.*, vol. 66, no. 1–3, pp. 355–360, 1998.

[4] J. Choi and C. Ahn, "Active microfluidic mixer for mixing of microparticles and liquids," in *Proc. SPIE*, vol. 4177, Microfluidic Devices and Systems III, Aug. 2000, pp. 154–161.

[5] R. H. Liu, M. A. Stremler, K. V. Sharp, M. G. Olsen, J. G. Santiago, R. J. Adrian, H. Aref, and D. J. Beebe, "Passive mixing in a three-dimensional serpentine microchannel," *J. Microelectromech. Syst.*, vol. 9, no. 2, pp. 190–197, June 2000.

[6] Z. Yang, S. Matsumoto, H. Goto, M. Matsumoto, and R. Maeda, "Ultrasonic micromixer for microfluidic systems," *Sens. Actuators A, Phys.*, vol. 93, pp. 266–272, 2001.

[7] M. Barbic, J. J. Mock, A. P. Gray, and S. Schultz, "Electromagnetic micromotor for microfluidics applications," *Appl. Phys. Lett.*, vol. 79, pp. 1399–1401, 2001.

[8] L.-H. Lu, K. S. Ryu, and C. Liu, "A magnetic microstirrer and array for microfluidic mixing," *J. Microelectromech. Syst.*, vol. 11, no. 5, pp. 462–469, Oct. 2002.

[9] A. D. Stroock, S. K. W. Dertinger, A. Ajdari, I. Mezic, H. A. Stone, and G. M. Whitesides, "Chaotic mixer for micro channels," *Science*, vol. 295, no. 5555, pp. 647–651, 2002.

[10] G. A. Mensing, T. M. Pearce, M. D. Graham, and D. J. Beebe, "An externally driven magnetic microstirrer," *Phil. Trans.: Math., Phys. Eng. Sci.*, vol. 362, pp. 1059–1068, Mar. 11, 2004.

[11] K. S. Ryu, K. Shaikh, E. Goluch, Z. Fan, and C. Liu, "Micro magnetic stir-bar mixer integrated with parylene microfluidic channels," *Lab on a Chip*, vol. 4, no. 6, pp. 608–613, 2004.

[12] W. Zhang and C. H. Ahn, "A bidirectional magnetic micropump on a silicon wafer," in *Proc. IEEE Solid-State Sensor and Actuator Workshop*, Hilton Head, SC, Jun. 2–6, 1996, pp. 94–97.

[13] D. Maillefer, H. Van Lintel, G. Rey-Mermet, and R. Hirschi, "A high-performance silicon micropump for an implantable drug delivery system," in *Proc. 12th IEEE MEMS Workshop*, Orlando, FL, 1999, pp. 541–546.

[14] K.-S. Yun, I.-J. Cho, J.-U. Bu, C.-J. Kim, and E. Yoon, "A surface-tension driven micropump for low-voltage and low-power operations," *J. Microelectromech. Syst.*, vol. 11, no. 5, pp. 454–461, Oct. 2002.

[15] J. W. Munyan, H. V. Fuentes, M. Draper, R. T. Kelly, and A. T. Woolley, "Electrically actuated, pressure-driven microfluidic pumps," *Lab on a Chip*, vol. 3, no. 4, pp. 217–220, October 8, 2003.

[16] N.-T. Nguyen and T.-Q. Truong, "A fully polymeric micropump with piezoelectric actuator," *Sens. Actuators, B, Chem.*, vol. 97, no. 1, pp. 137–143, 2004.

[17] J. Atencia and D. J. Beebe, "Magnetically-driven biomimetic micro pumping using vortices," *Lab on a Chip*, vol. 4, no. 6, pp. 598–602, 2004.

[18] D. J. Beebe, J. S. Moore, Q. Yu, R. H. Liu, M. L. Kraft, B.-H. Jo, and C. Devadoss, "Microfluidic tectonics: a comprehensive construction platform for microfluidic systems," *PNAS*, vol. 97, no. 25, pp. 13 488–13 493, Dec. 5, 2000.

[19] A. K. Agarwal, S. S. Sridharamurthy, T. M. Pearce, G. A. Mensing, D. J. Beebe, and H. Jiang, "Magnetically-driven actuation using liquid-phase polymerization (LPP) and its application: a programmable mixer," in *Proc. Hilton Head: A Solid State Sensor, Actuator, and Microsystem Workshop*, Hilton Head Island, SC, Jun. 6–10, 2004, pp. 121–124.

[20] A. K. Agarwal, J. Atencia, D. J. Beebe, and H. Jiang, "Magnetically-driven temperature-controlled microfluidic actuators," in *Proc. 1st Int. Workshop on Networked Sensing Syst.*, Tokyo, Japan, Jun. 22–23, 2004, pp. 51–55.

[21] S. Metz, R. Holzer, and P. Renaud, "Polyimide-based microfluidic devices," *Lab on a Chip*, vol. 1, no. 1, pp. 29–34, 2001.

[22] D. J. Beebe, J. S. Moore, J. M. Bauer, Q. Yu, R. H. Liu, C. Devadoss, and B.-H. Jo, "Functional hydrogel structures for autonomous flow control inside microfluidic channels," *Nature*, vol. 404, pp. 588–590, 2000.

[23] D. T. Eddington and D. J. Beebe, "Flow control with hydrogels," *Adv. Drug Del. Rev.*, vol. 56, no. 2, pp. 199–210, Feb. 10, 2004.

[24] ——, "A valved responsive hydrogel microdispensing device with integrated pressure source," *J. Microelectromech. Syst.*, vol. 13, no. 4, pp. 586–593, August 2004.

[25] A. Richter, D. Kuckling, S. Howitz, T. Gehring, and K.-F. Arndt, "Electronically controllable microvalves based on smart hydrogels: magnitudes and potential applications," *J. Microelectromech. Syst.*, vol. 12, no. 5, pp. 748–753, 2003.

[26] H. J. Van der Linden, W. Othuis, and P. Bergveld, "An efficient method for the fabrication of temperature-sensitive hydrogel microactuators," *Lab on a Chip*, vol. 4, pp. 619–624, 2004.

[27] A. Suzuki and T. Tanaka, "Phase transition in polymer gels induced by visible light," *Nature*, vol. 346, pp. 345–347, 1990.

[28] K. K. Lee, E. L. Cussler, M. Marchetti, and M. A. McHugh, "Pressure-dependent phase transition in hydrogels," *Chem. Eng. Sc.*, vol. 45, no. 3, pp. 766–767, 1990.

[29] T. Miyata, N. Asami, and T. A. Uragami, "A reversibly antigen-responsive hydrogel," *Nature*, vol. 399, pp. 766–769, 1999.

[30] T. Tanaka, I. Nishio, S.-T. Sun, and S. Ueno-Nishio, "Collapse of gels in an electric fields," *Science*, vol. 218, pp. 467–469, 1982.

[31] M. J. Bassetti, A. N. Chatterjee, N. R. Aluru, and D. J. Beebe, "Development and modeling of electrically triggered hydrogels for microfluidic applications," *J. Microelectromech. Syst.*, vol. 14, no. 5, pp. 1198–1207, Oct. 2005.

[32] Y. Li and T. Tanaka, "Kinetics of swelling and shrinking of gels," *J. Chem. Phys.*, vol. 92, no. 2, pp. 1365–1371, 1990.

[33] S. H. Gehrke, "Synthesis, equilibrium swelling, kinetics, permeability and applications of environmentally responsive gels," in *Responsive Gels: Volume Transitions II*, K. Dusek, Ed. Heidelberg, Germany: Springer-Verlag, 1993, vol. 110, Advances in Polymer Science, pp. 81–144.

[34] Q. Yu, *Development of Functional Polymeric Materials for Microfluidic Systems*. Urbana, IL: Department of Chemistry, University of Illinois at Urbana-Champaign, 2002, pp. 3–11.

[35] H. Kawasaki, S. Sasaki, H. Meada, and K. Nishinari, "Effect of introduced charge on the thermal behavior of *N-isopropylacrylamide* gels in water and NaCl solutions," *Langmuir*, vol. 16, pp. 3195–3199, 2000.

[36] *Microfab NI 100 Data Sheet*. West Haven, CT: Enthone-OMI Inc., Jul. 2000.

[37] J. Zou, C. Liu, J. Schutt-Aine, J. Chen, and S.-M. Kang, "Development of a wide tuning range MEMS tunable capacitor for wireless communication systems," in *Proc. IEDM*, Dec. 10–13, 2000, pp. 403–406.

[38] M. Koch, H. Witt, G. Evans, and A. Brunnschweiler, "Improved characterization technique for micromixers," *J. Micromech. Microeng.*, vol. 9, pp. 156–158, 1999.

Abhishek K. Agarwal received the B.S. degree in electrical and computer engineering from the University of Illinois at Urbana-Champaign in 2000 and the M.S. degree in electrical and computer engineering from the University of Wisconsin-Madison in 2003.

He is currently pursuing the Ph.D. degree in electrical and computer engineering from the University of Wisconsin-Madison. His research interests include the development of integrated microfluidics and MEMS to realize programmable autonomous microfluidic systems (temperature control systems and liquid microlens) and building block components (micro-mixers and pumps).

Sudheer S. Sridharamurthy received the B.E. degree in electronics and communication from the University of Mysore, India, in 1999 and the M.Tech. degree in electronics design and technology from the Indian Institute of Science in 2002. He is currently pursuing the Ph.D. degree in electrical and computer engineering from the University of Wisconsin-Madison.

His research interests include developing efficient sensing mechanisms for biological species, electronic interface circuits for sensors, and microfluidics.

David J. Beebe (S'89–M'95) received the B.S., M.S., and Ph.D. degrees in electrical engineering from the University of Wisconsin-Madison in 1987, 1990, and 1994, respectively.

He is a Professor in the Department of Biomedical Engineering at the University of Wisconsin-Madison. He is also a member of the the University of Wisconsin (UW) Comprehensive Cancer Center, Stem Cell Program, Materials Science Program, Biotechnology Training Program, Genomic Sciences Training Program and serves on the steering committee of the Stem Cell Training Program. From 1996 to 1999, he was an Assistant Professor in the Department of Electrical and Computer Engineering and an Assistant Research Professor in the Beckman Institute for Advanced Science and Technology at the University of Illinois at Urbana-Champaign. From 1994 to 1996, he was an Assistant Professor at Louisiana Tech University, Baton Rouge. His current interests center around understanding the role stem/progenitor cells play in the development of the mammary gland.

Dr. Beebe is the recipient of the IEEE EMBS Early Career Achievement Award and the Romnes Award at UW-Madison.

Hongrui Jiang (S'98–M'02) received the B.S. degree in physics from Peking University, Beijing, China. He received the M.S. and Ph.D. degrees in electrical engineering from Cornell University, Ithaca, NY, in 1999 and 2001, respectively.

He is currently an Assistant Professor with Department of Electrical and Computer Engineering and a Faculty Affiliate with the Department of Biomedical Engineering at University of Wisconsin-Madison (UW-Madison). His research focuses on microfabrication technology, biological and chemical microsensors, microactuators and microfluidics. Before he joined the faculty of UW-Madison in 2002, he was a Postdoctoral Researcher at the Berkeley Sensor and Actuator Center, University of California, Berkeley, from 2001 to 2002.